ChemMedChem

Chemistry Europe
European Chemical Societies Publishing

Accepted Article

Title: The Stone Guest: How Does pH Affect Binding Properties of PD-1/PD-L1 Inhibitors ?

Authors: Alessandra Riccio, Alice Coletti, Daniela Dolciami, Andrea Mammoli, Bruno Cerra, Sonia Moretti, Antimo Gioiello, Simone Ferlin, Efisio Puxeddu, and Antonio Macchiarulo

To be cited as: *ChemMedChem* 10.1002/cmdc.202000760

Link to VoR: https://doi.org/10.1002/cmdc.202000760

WILEY-VCH

WILEY-VCH

FULL PAPER

The Stone Guest: How Does pH Affect Binding Properties of PD-1/PD-L1 Inhibitors ?

Dr. Alessandra Riccio,[a] Dr. Alice Coletti,[b] Dr. Daniela Dolciami,[a] Dr. Andrea Mammoli,[a] Dr. Bruno Cerra,[a] Dr. Sonia Moretti,[b] Prof. Antimo Gioiello,[a] Dr. Simone Ferlin,[c] Prof. Efisio Puxeddu,[b] Prof. Antonio Macchiarulo.*[a]

[a] Dr. A. Riccio, Dr. D. Dolciami, Dr. A. Mammoli, Dr. B. Cerra, Prof. A. Gioiello, Prof. A. Macchiarulo, ORCID:0000-0001-9535-4183
Department of Pharmaceutical Sciences
University of Perugia,
via del liceo n.1, 06123 – Perugia (Italy)
E-mail: antonio.macchiarulo@unipg.it
[b] Dr. A. Coletti, Dr. S. Moretti, Prof. E. Puxeddu
Department of Medicine,
University of Perugia,
via Gambuli, 1 – 06132, Perugia (Italy).
[c] Dr. S. Ferlin
Sterling S.p.A.,
Via della Carboneria, 30 – 06073, Corciano (Perugia, Italy).

Supporting information for this article is given via a link at the end of the document.

Abstract: The interaction between programmed cell death-1 (PD-1) and its ligand PD-L1 activates a coinhibitory signal that blocks T-cell activation, promoting the immune escape process in the tumor microenvironment. Development of monoclonal antibodies targeting and inhibiting PD-1/PD-L1 interaction as anticancer immunotherapies has proved successful in multiple clinical settings and for various types of cancer. Notwithstanding, limitations exist with the use of these biologics, including drug resistance and narrow therapeutic response rate in a majority of patients, that demand for the design of more efficacious small molecule-based immunotherapies. Alteration of pH in the tumor microenvironment is a key factor that is involved in promoting drug resistance, tumor survival and progression. In this study, we have investigated the effect of pH shifts on binding properties of distinct classes of PD-L1 inhibitors, including macrocyclic peptide and small molecules. Results expand structure-activity relationships of PD-L1 inhibitors, providing insights into structural features and physicochemical properties that are useful for the design of ligands that may escape a drug resistance mechanism associated to variable pH conditions of tumor microenvironment.

Introduction

Programmed cell death-1 protein (PD-1) and its ligands (PD-L1 and PD-L2) are members of the B7–CD28–CTLA-4 family of coregulatory proteins which play a pivotal role in T-cell activation and tolerance.[1-3]

Structurally, PD-1 is a monomeric type I transmembrane glycoprotein containing an IgV extracellular domain, followed by a stalk region of about 20 amino acids and a cytoplasmic domain.[4] This latter bears tyrosine-based motifs called Immunoreceptor Tyrosine-based Inhibitory Motif (ITIM) and Immunoreceptor Tyrosine-based Switch Motif (ITSM).[5] The engagement of PD-1 by its ligand PD-L1 promotes the phosphorylation of the ITSM motif and the formation of a docking site which is able to recruit SHP-1 and SHP-2, leading to the inhibition of T cells activity. At odds with other B7–CD28–CTLA-4 proteins, PD-1 is mostly expressed on T and B cells, natural killer (NK) and monocytes, suggesting a wider regulation of immune responses than other family members.[6,7]

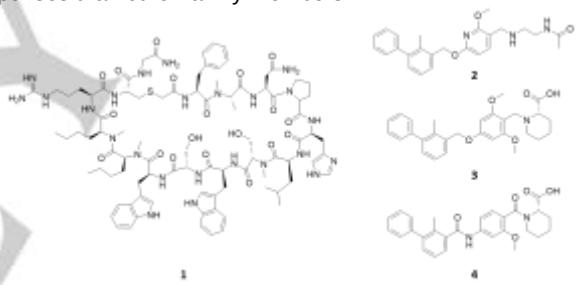

Figure 1. Chemical structures of peptide-57 (**1**, S8158), BMS-202 (**2**), S7911 (**3**) and VIS1059 (**4**).

PD-L1 and PD-L2 share 20% of sequence identity with other members of the B-7 family.[8] They are type I transmembrane glycoproteins composed of a membrane-proximal Ig-C and a membrane-distal Ig-V-type ectodomain.[9] The Ig-V domain consists of antiparallel β-strands which form two possible interaction surfaces, termed GFC and BED surface. The interaction between PD-L1/2 and PD-1 occurs at the GFC surface, which is different in the two ligand proteins accounting for a distinct molecular mechanism of interaction.[10-13] In particular, PD-L1 and PD-L2 compete for the same binding surface on PD-1. However, upon binding, the larger GFC surface of PD-L1 induces a peculiar conformational change in PD-1 that is not observed in the case of PD-L2. Such different molecular mechanism of interaction may account for a 3-fold lower affinity of PD-L1 than PD-L2 to PD-1.[14]

Among PD-1 ligands, PD-L1 is highly present in tumor cells, with its expression being induced by many cytokines and tumor-derived exosomes. It is also constitutively expressed in antigen presenting cells (APCs), T-cells and on a variety of non-hematopoietic cell types.[15] On this basis, recent studies suggest that PD-L1 may constitute a key factor for triggering the promotion

of the immune escape process in the tumor microenvironment.[16, 17] Accordingly, inhibition of PD-1/PD-L1 interaction is being pursued as viable strategy to develop anticancer immunotherapies, engineering humanized monoclonal antibodies or designing peptidomimetics and small molecule inhibitors.[18] In this framework, the use of PD-1/PD-L1 humanized monoclonal antibodies has yielded 20%-50% positive response rates in multiple clinical trials and for various types of cancer, evidencing that a significant portion of patients shows drug resistance and poor therapeutic response.[19-21]

Beyond limited bioavailability and safety issues of biologic drugs, the lack of a wider response to PD-1/PD-L1 monoclonal antibodies has been correlated to low tumor-infiltrating immune cells, absence of activated effector T cells, and poor PD-L1 expression in cancer cells, which collectively constitute the dynamic cell content profile of a tumor microenvironment.[22] Spatiotemporal alteration of pH in tumor microenvironment is another factor that has been reported to promote tumor survival and progression, and may contribute to establish drug resistance towards anticancer therapies.[23, 24] Specifically, normal tissues present an intracellular pH (pHi) of 7.2, and an extracellular pH (pHe) of 7.4. In tumor microenvironment, pHe decreases to acidic values below 7.0, while pHi assumes higher basic values.[25-27] These changes can alter the ratio of protonated versus deprotonated forms of charged residues on target proteins and chemical groups on cognate ligands, depending on the relative acid dissociation constants (pKa). Accordingly, shifts of pHi/pHe out of the physiological range can affect both target protein functionality as well as drug efficacy, weakening electrostatic interactions which govern protein structure, folding and ligand binding.[28]

In this work, we attempt to investigate the effect of pH variations on binding properties of a selection of PD-L1 inhibitors belonging to the different chemical categories of macrocyclic peptides and small molecule inhibitors (**1**-**4**, Figure 1). Firstly, docking studies and molecular dynamic (MD) simulations were carried out to depict putative electrostatic interactions and hydrogen bonds featuring the binding modes of these inhibitors to PD-L1. Next, analysis of physicochemical properties was carried out to assess pKa values of aminoacidic residues and small molecules. Finally, microscale thermophoresis (MST) analysis was performed to evaluate dissociation constants (K_d) of inhibitors to PD-L1 at different pH conditions.

Results and Discussion

Binding modes of inhibitors to PD-L1.

A selection of inhibitors of PD-L1 belonging to chemical classes of macrocyclic peptides and small molecules was collected from literature, including peptide-57 (**1**, S8158; pdb code 5O4Y), BMS-202 (**2**, pdb code: 5J89) and S7911 (**3**). A further compound (**4**, VIS1059) was ad-hoc designed and synthetized as structural analogue of S7911, but endowed with different protonation state and conformational property.

Peptide-57 (**1**) is a macrocyclic compound that is able to block PD-1/PD-L1 interaction with an EC_{50} of 0.566 ± 0.122 μM, as determined in a luciferase reporter assay using T-cell-like Jurkat cells.[29] Crystallographic studies have shown that peptide-57 binds to the GFC surface of PD-L1, mostly engaging the G strand of the target protein by hydrophobic interactions (Figure 2).

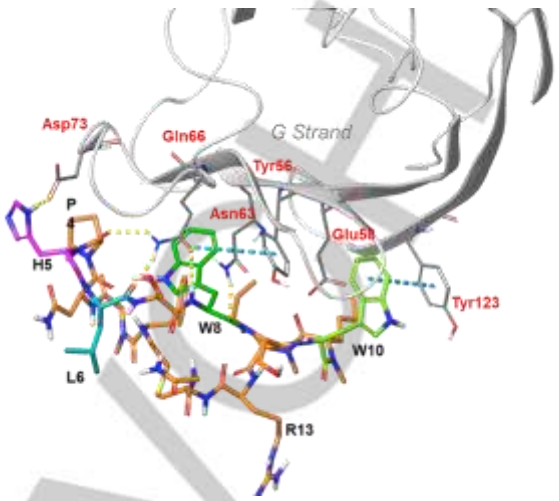

Figure 2. Interactions of peptide-57 (**1**) on the GFC surface of PD-L1 (5O4Y). Yellow dashed lines show ligand/target hydrogen bond interactions; cyan dashed lines show ligand/target π-stacking contacts.

Table 1. Stabilities (occupancy, %) of ligand/protein interactions as resulting from trajectories of MD simulations.

Resid.	Inter. Type	**2**/PD-L1 (5J89 C/D)	**3**/PD-L1 (5J89 C/D)	**4**/PD-L1 (5J89 C/D)	**1**/PD-L1 (504Y)
Phe19	H-bond[a]	32% C[e]	-	-	-
Glu58	H-bond	-	-	-	68%
Asn63	H-bond	-	-	-	100%
Gln66	H-bond	-	-	62% D[e]	252%
Asp73	H-bond	-	-	-	32%
Asp122	H-bond	65% C	35% C	-	-
Lys124	H-bond	35% C	65% C	-	-
Glu58	Water[b]	-	-	-	40%
Asn63	Water	-	-	-	32%
Gln66	Water	-	-	61% D	-
Asp73	Water	-	-	-	81%
Val76	Water	-	-	-	30%
Ala121	Water	58% C	-	-	-
Asp122	Water	30% C	-	-	-
Phe19	Water	63% C	-	31% C	-
Thr20	Water	-	37% C	-	-
Tyr56	phobic[c]	40% D	47% D	58% D	48%
Val68	phobic	-	36% D	-	31%
Ile54	phobic	46% D	-	-	-
Met115	phobic	38% D	-	39% D	41%
Ala121	phobic	43% C	31% C	36% C	-
Tyr123	phobic	64% C	45% C	32% D	56%
Tyr56	π-π[d]	67% C/D[e]	66% C/D	76% C/D	-

[a] H-bond: hydrogen bond; [b] Water: water-bridge mediate hydrogen bond; [c] phobic: hydrophobic contacts; [d] π-π: π-interaction; [e] protein chain C and/or D of PD-L1 dimeric form.

Specifically, tryptophan residues (W8 and W10) of peptide-57 occupy two narrow clefts of PD-L1, making hydrophobic contacts and π-stacking interactions with Ile54, Tyr56 and Val68 in the first

cleft, and Tyr56, Glu58, Arg113, Met115 and Tyr123 in the second cleft. Furthermore, two hydrogen bond interactions are observed between the side chain of Gln66 and backbone atoms of L6 and W10, while one additional hydrogen bond is formed between Asn63 and the backbone carbonyl of W8.

MD simulation provides insights into relative stabilities of these interactions (Table 1). In particular, hydrogen bond interactions involving P4, L6, and W8 of peptide-57, and the backbone of Gln66 and Asn63 of PD-L1 show a very high stability along the trajectory (Table 1; occupancy values 252% and 100%, respectively). These are followed by a further stable hydrogen bond involving residues W10 and Glu58 (occupancy 68%), and by both water-bridge mediated and direct hydrogen bond interactions connecting H5 and Asp73 (occupancy 81%, 32%). Stable hydrophobic contacts and π-stacking interactions are observed between Met115, Tyr123 and Tyr56, and F1, W8 and W10 of peptide-57. Noteworthy, the basic residue R13 of peptide-57 is not directly engaged in any polar interaction with specific residues of PD-L1, but it is exposed to solvent molecules. Although MD simulation confirms hydrophobic interactions as important in the binding of peptide-57 to the GFC surface of PD-L1, it also pinpoints a significant contribution of polar interactions to the stability of the complex.

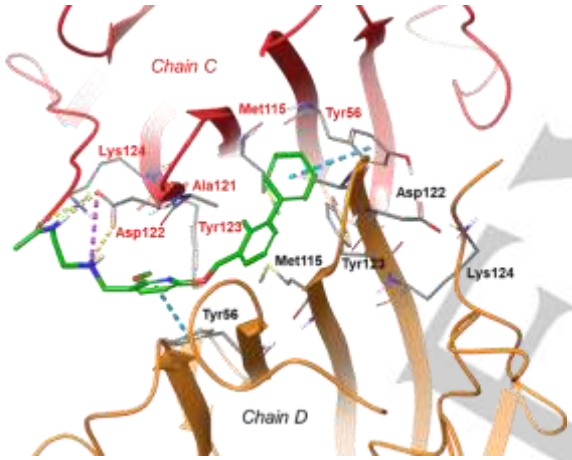

Figure 3. Interactions of BMS-202 (**2**) into the binding cleft of the dimeric form of PD-L1 (5J89). Yellow dashed lines show ligand/target hydrogen bond interactions; cyan dashed lines show ligand/target π-stacking contacts; purple dashed lines show ligand/target electrostatic interactions.

BMS-202 (**2**) belongs to a class of (2-methyl-3-biphenylyl)methanol derivatives identified by Bristol-Myers Squibb as small molecule inhibitors of PD-L1/PD-1 interaction,[30] with an IC50 of 0.018 μM in homogeneous time-resolved fluorescence (HFRET) binding assay. The determination of the crystal structure of BMS-202 in complex with PD-L1 has allowed to get insights into the mechanism of interaction of this class of small molecules.[31] Specifically, it was found that BMS-202 induces a dimeric form of PD-L1, binding into a cavity shaped by the GFC surface of two PD-L1 units (Figure 3). The biphenyl moiety of **2** is buried within the cavity engaging Met115 and Ala121 of both PD-L1 chains (e.g. chains C/D) with hydrophobic contacts, while its distal phenyl ring makes π-stacking interactions with Tyr56 of chain C. The pyridine ring forms a π-stacking interaction with Tyr56 of chain D, and its methoxy substituent makes hydrophobic contacts with Tyr123 of chain C. The terminal 2-aminoethylacetamide chain of BMS-202 protrudes into the solvent with its secondary amine and acetamido groups facing a salt bridge formed by the side chains of Asp122 and Lys124 of chain C.

The MD simulation shows strong stability of the above π-stacking interactions with Tyr56 (Table 1; chains C and D, occupancy 67%), and hydrophobic contacts with Tyr123 (chain C, occupancy 64%). Moreover, water-bridge mediated hydrogen bonds are observed between the backbone of Phe19, Ala121 and the secondary amine group of BMS-202 along the MD trajectory (chain C, occupancy 63%, 58%). Noteworthy, the secondary amine group and the nitrogen atom of the amide moiety make stable hydrogen bond interactions with the side chain of Asp122 (chain C, occupancy 65%). The carbonyl group of the acetamide moiety is involved in hydrogen bond interaction with the side chain of Lys124 (chain C, occupancy 35%).

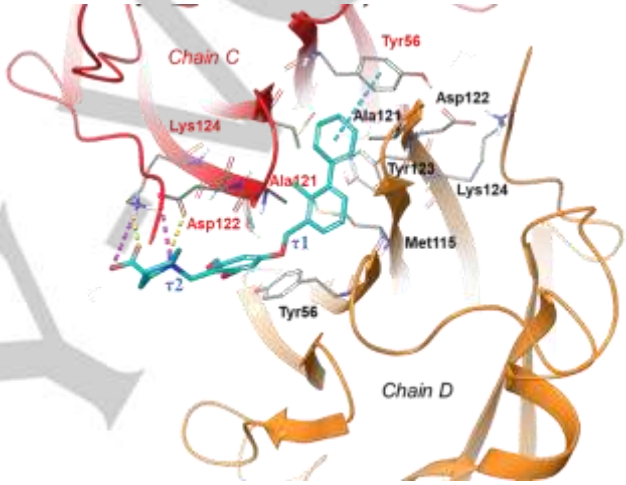

Figure 4. Interactions of S7911 (**3**) into the binding cleft of the dimeric form of PD-L1 (5J89). Yellow dashed lines show ligand/target hydrogen bond interactions; cyan dashed lines show ligand/target π-stacking contacts; purple dashed lines show ligand/target electrostatic interactions. Torsional ether angle (τ1 = 156±17°) and amine angle (τ2 = 162±29°) are labelled.

No crystallographic studies are available for S7911 (**3**) and its analogue (**4**, VIS1059). Accordingly, docking studies were carried out using the dimeric crystal structure of PD-L1 (pdb code: 5J89) followed by MD simulations (Figure 4). Akin to BMS-202 (**2**), S7911 (**3**) engages the GFC surface of two PD-L1 units with a binding mode that is characterized by stable aromatic interactions between its biphenyl moiety and Tyr56 (Table 1; chains C/D, occupancy 66%), as well as hydrophobic contacts with Ala121 (chain C; occupancy 31%). A salt bridge interaction is observed between the negatively charged group of Asp122 and the protonated ternary amine group of **3** (chain C, occupancy 35%), whereas the side chain of Lys124 makes both salt bridge and hydrogen bond interactions with the carboxylate group of the compound (chain C, occupancy 65%). Compound VIS1059 (**4**) was designed as distant analogue of S7911 (**3**), replacing the ternary amine and central ether core of the latter compound with two amide moieties. These replacements allow restraining the conformational freedom of two dihedral angles due to the energetic favored planar geometry of the amide torsional angle with respect to the ether (τ1) and amine (τ2) torsional angles. Nearly anti-planar conformations of the ether angle (τ1 = 156±17°) and amine angle (τ2 = 162±29°) are indeed observed along the

MD trajectory of S7911. Furthermore, the conversion of the amine nitrogen to an amide nitrogen bestows a different protonation state to the derived compound. Docking and MD simulation reveals conserved aromatic interactions between the biphenyl moiety of the analogue **4** and Tyr56 (Table 1, chains C/D; occupancy 76%), as well as hydrophobic contacts with Ala121 (chain C, occupancy 36%). Stable hydrogen bonds are formed between the side chain of Gln66 and the carbonyl group of the terminal amide moiety (chain D, occupancy 62%). An additional water-bridge mediated hydrogen bond is observed between the side chain of Gln66 (chain D, occupancy 61%) and the carbonyl group of analogue **4**.

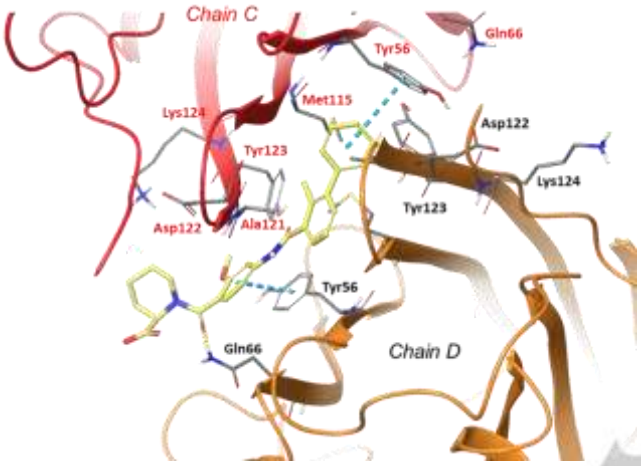

Figure 5. Interactions of VIS1059 (**4**) into the binding cleft of the dimeric form of PD-L1 (5J89). Yellow dashed lines show ligand/target hydrogen bond interactions; cyan dashed lines show ligand/target π-stacking contacts.

Synthesis of VIS1059.

The synthesis of compound VIS1059 (**4**) was realized according to Scheme 1. In particular, methyl-[1,1'-biphenyl]-3-yl)methanol (**5**) was converted into the corresponding carboxylic acid derivative **6** by oxidation reaction with sodium bromate (3 equiv.) and sodium hydrogen sulfate (1 equiv.) in refluxing MeCN.[32]

The acid **6** obtained in 70% yield was reacted with oxalyl chloride in dry CH2Cl2/DMF at room temperature and the acyl chloride thus formed was readily treated with 4-amino-2-methoxybenzoic acid in the presence of Et3N to form the desired 2-methoxy-4-(2-methyl-[1,1'-biphenyl]-3-carboxamido)benzoic acid (**7**) in 8% isolated yield.

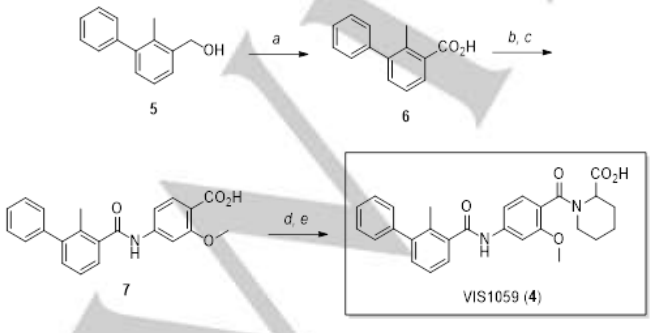

Scheme 1. Synthesis of VIS1059 (**4**). Reagents and conditions: a) $NaBrO_3$, $NaHSO_4$, MeCN, reflux, 70%; b) $(COCl)_2$, CH_2Cl_2, DMF, r.t.; c) 4-amino-2-methoxybenzoic acid, Et_3N, CH_2Cl_2, r.t., 8% from 6; d) $(COCl)_2$, dry CH_2Cl_2, DMF, r.t.; e) pipecolic acid, Et_3N, CH_2Cl_2, r.t., 8% from **7**.

Treatment of **7** with oxalyl chloride and Et3N in dry CH2Cl2/DMF followed by reaction with a slight excess of pipecolic acid (1.05 equiv.) afforded VIS1059 (**4**) in 8% yield.

Physicochemical properties.

Calculated and experimental acidic constants (cpKa, pKa) were assessed for the macrocyclic peptide (**1**), small molecule inhibitors (**2**-**4**) and selected polar residues of PD-L1 (Table 2).

As a result, small molecules cover a different range of pKa values, and may assume diverse protonation states depending on the environmental pH condition. In particular, BMS-202 (**2**) bears a secondary amine group (cpKa2= 7.67/7.74; pKa2= 8.39±0.05) and a pyridine nitrogen (cpKa1= 0.64/1.48). While the latter group assumes an uncharged state, the protonated/unprotonated ratio of the amine group may be affected by changes of pHe and pHi values in the tumor microenvironment.[25-27]

S7911 (**3**) is an α-aminoacidic compound featuring a cyclic ternary amine group. According to its experimental pKa values (pKa1= 2.78 ± 0.08; pKa2= 10.49 ± 0.19), this compound mostly adopts a zwitterion form at physiological pHe values. VIS1059 (**4**) is an acidic compound (cpKa1= 3.44/3.65; pKa1= 4.77 ± 0.06) that assumes a deprotonated negatively charged state at physiological pHe value, whereas it may increasingly adopt a neutral uncharged state with decreasing pHe value in the tumor microenvironment.

Table 2. Calculated and experimental pKa properties of compounds **1**-**4** and selected residues of PD-L1 (Glu58, Asp73, Asp122 and Lys124).

Cpd./ Res.	cpKa1	cpKa2	cpKa3	pKa1	pKa2
1	6.74 [a] 7.18 [b]	11.80 [a] 11.49 [b]	>12.0 [a] >12.0 [b]	-	-
2	0.64 [a] 1.48 [b]	7.67 [a] 7.74 [b]	-	n.d.[c]	8.39±0.05
3	1.04 [a] 1.99 [b]	6.41 [a] 8.87 [b]	-	2.78±0.08	10.49±0.19
4	3.44 [a] 3.65 [b]	-	-	4.77±0.06	-
Glu58 [d]	3.1	-	-	-	-
Asp73 [d]	2.3	-	-	-	-
Asp122 [e]	<0.0	-	-	-	-
Lys124 [e]	>12.0	-	-	-	-

[a] Marvin pKa prediction; [b] Epik pKa prediction in water; [c] n.d. = not determined (out of the range of values of Sirius T3, pH 2-12); [d] calculated using 5O4Y structure; [e] calculated using 5J89 structure. Experimental pKa values are reported as mean ± standard deviation from n.3 titrations.

The macrocyclic peptide (**1**) has one arginine residue (R13) with a calculated cpKa of 11.80/11.49, and a histidine residue (H5) with calculated pKa values of 6.74/7.18 and >12.0. Hence, H5 assumes a protonated state with decreasing value of pHe in the tumor microenvironment, whereas the side chain of R13 stably adopts a protonated form. Acidic residues of PD-L1 that are in contact with the macrocyclic peptide (**1**) in the crystallographic complex (pdb code 5O4Y) are Glu58 (cpKa1= 3.1) and Asp73 (cpKa1= 2.3). Side chains of these residues are exposed to the solvent and mostly adopt a deprotonated negatively charged state at the pHe of the tumor microenvironment. In the crystallographic complex of BMS-202 (**2**) bound to PD-L1 (pdb code 5J89), acidic and basic residues in contact with the ligand include Asp122 (cpKa< 0.0) and Lys124 (cpKa> 12.0) that engage each other in a salt bridge interaction. Accordingly, the carboxylic group of Asp122 assumes a deprotonated form whereas the primary

amine group of Lys122 adopts a positively charged state at any pHe of the tumor microenvironment.

Effect of pH on dissociation constants of PD-L1 inhibitors.
Since the selected inhibitors (**1**-**4**) have different binding modes and physicochemical properties, in this part of the study we investigated how and how much shifts of pH affect their binding properties to PD-L1. Ligand binding assays were thus performed using microscale thermophoresis (MST). Thermophoresis is the movement of a biomolecular complex in a temperature gradient depending on size, charge, and hydration shell that typically change upon ligand/target interaction.[33] In combination with cellular and other biochemical assays, this approach was previously used to investigate the target engagement of a selected set of PD-1/PD-L1 inhibitors which included peptide-57 (**1**) and other small-molecule inhibitors. In particular, authors found that peptide-57 (**1**) and two analogues of BMS-202 (**2**) were able to bind to PD-L1 in the nanomolar range of potency.[34] Binding properties of PD-L1 inhibitors were assessed at three different pH values (pH = 6.2, 7.2, 8.2), above the theoretical isoelectric point of the protein (pI = 5.73). Stability of unlabelled and labelled recombinant protein at the three different pH values was checked using thermal shift assays (Figure S1 and Table S1, supplementary material). Results show very similar unfolding profiles and Ti values of the protein, suggesting that labelling and different pH conditions do not affect the proper folding of PD-L1.
The binding of compounds **1**-**4** to fluorescently labelled PD-L1 (red-hPD-L1) was firstly evaluated at pH 7.2. As a result, compounds 1-3 yield a productive binding interaction to PD-L1 (Figures 6-8), whereas no binding activity is observed for VIS1059 at tested concentrations (**4**, Figure 9; K_d > 1mM).

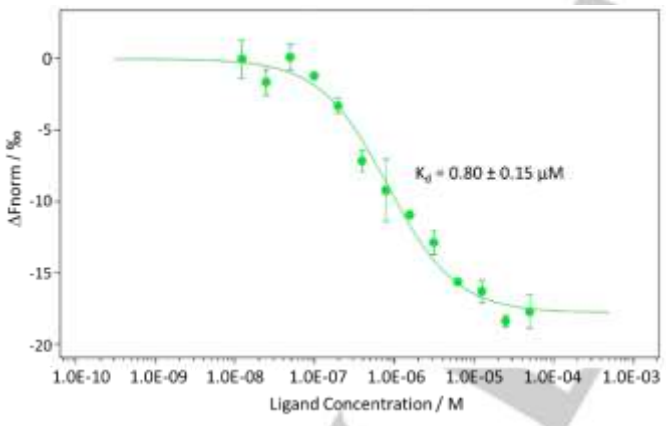

Figure 6. MST binding curve of peptide-57 (1) to red labelled recombinant human PD-L1 at pH 7.2 condition. The binding curve and K_d ± c.v value were generated from n.3 independent experiments.

This finding pinpoints that presence of a negative net charge on the molecule (pKa1= 4.77 ± 0.06) is detrimental for the interaction to PD-L1, and aromatic as well as hydrophobic contacts between the biphenyl moiety of **4** and binding site residues are unable to compensate for it. Noteworthy, in the MD simulation the carboxylic group of VIS1059 (**4**) does not form any specific salt bridge interaction with the nearby positively charged Lys124, as instead observed for its α-aminoacidic analogue **3**. This is also in agreement with statistical studies suggesting that binding sites of carboxylic groups have mostly two polar residues with two hydrogen bond donors to make stable interactions.[35]

Moreover, it is possible that conformational restraining upon amide group insertion may be detrimental for the binding activity of **4**. Peptide-57 (**1**) results the most potent PD-L1 ligand among tested compounds, generating a dissociation constant (K_d) value of 0.80 ± 0.15 µM with a negative thermophoretic trend (Figure 6).

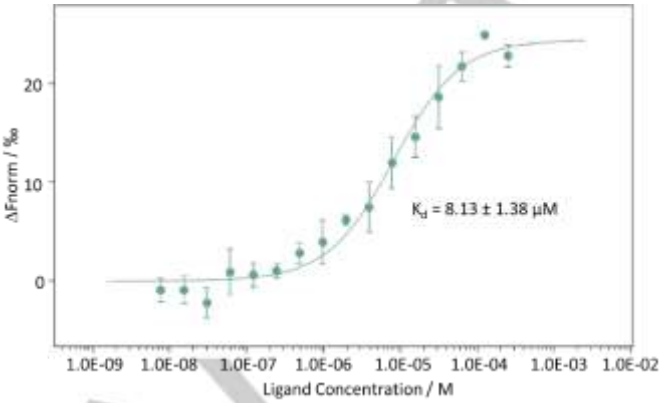

Figure 7. MST binding curve of BMS-202 (**2**) to red labelled recombinant human PD-L1 at pH 7.2 condition. The binding curve and K_d ± c.v value were generated from n.3 independent experiments.

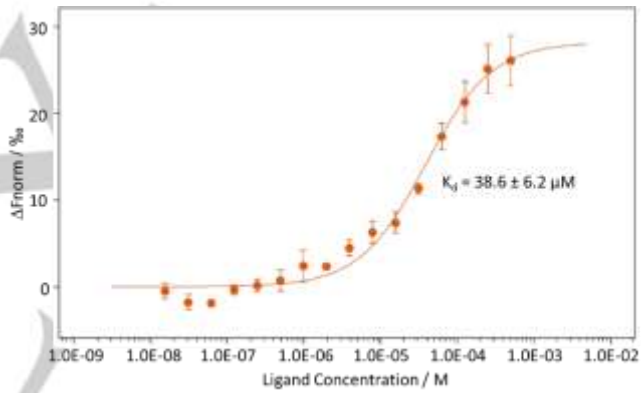

Figure 8. MST binding curve of S7911 (**3**) to red labelled recombinant human PD-L1 at pH 7.2 condition. The binding curve and K_d ± c.v value were generated from n.3 independent experiments.

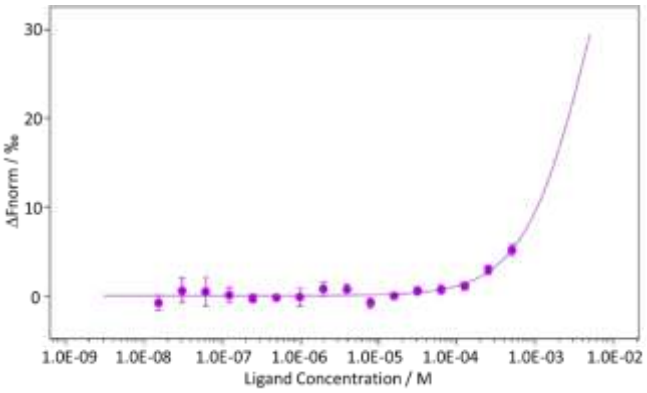

Figure 9. MST binding curve of VIS1059 (**4**) to red labelled recombinant human PD-L1 at pH 7.2 condition. The binding curve was generated from n.3 independent experiments.

Previous MST studies reported a K_d value of 0.019 ± 0.002 µM for this compound.[34] Discrepancy between the two results, however, can be explained by the use of different experimental settings in

the two studies (e.g. labeling protocols, time of measurements, type of capillaries). According to a rank order of binding potency, peptide-57 (**1**) is followed by BMS-202 (**2**; K_d = 8.13 ± 1.38 μM) and S7911 (**3**; K_d = 38.6 ± 6.2 μM), with these compounds showing a positive thermophoretic trend (Figures 7, 8). Hence, at the opposite of VIS1059 (**4**), presence of a positive net charge in BMS-202 (**2**) favors the binding activity to PD-L1, while the neutral net charge of the zwitterionic group in S7911 (**3**) produces a slightly decrease of potency. Remarkably, the positive thermophoretic trend of small molecules (**2**, **3**) and the negative thermophoretic trend of macrocyclic peptide (**1**) may be ascribed to a distinct mechanism of interaction of these classes of ligands to PD-L1, with small molecules inducing a dimerization form of the protein whereas macrocyclic peptide binding to a monomeric form of PD-L1.[36]

Next, binding activities of compounds **1**-**3** to PD-L1 were evaluated at pH 6.2 and 8.2, with results being reported in table 3. Inspection of the table reveals that the dissociation constant of peptide-57 (**1**) is marginally affected by the shift of pH conditions, with only pH 6.2 producing a slight improvement of the binding activity (K_d = 0.38 ± 0.07 μM).

Table 3. Dissociation constants (Kd) of compounds **1**-**3** against PD-L1 at different pH conditions.

Cpd.	pH 6.2 K_d ± c.v.[a]	pH 7.2 K_d ± c.v.	pH 8.2 K_d ± c.v.
1	0.38 ± 0.07 μM	0.80 ± 0.15 μM	0.84 ± 0.13 μM
2	4.50 ± 0.56 μM	8.13 ± 1.38 μM	12.37 ± 1.91 μM
3	33.5 ± 4.6 μM	38.6 ± 6.2 μM	57.3 ± 11.8 μM

[a] c.v.: confidence values. K_d ± c.v values were generated from n.3 independent experiments.

This observation is in agreement with previous studies reporting hydrophobic contacts of **1** rather than electrostatic interactions as important for macrocyclic peptide binding to PD-L1. However, the slight improvement of the binding activity of peptide-57 finds a likely explanation in the presence of a histidine residue (H5; cpKa= 6.74) whose fraction of protonated form becomes the major microspecies at pH 6.2. As a consequence, the hydrogen bond interaction observed in the MD simulation between H5 and Asp73 (Table 1, Figure 2) would be enforced by an energetically stronger salt bridge interaction.

The analysis shows that BMS-202 (**2**) is affected by the pH condition, with lower and higher pH values strengthening and weakening the interaction to PD-L1, respectively. This observation reflects the protonation state of the secondary amine group of 2, with its pKa value (pKa2= 8.39 ± 0.05) standing at the edge of the pH range adopted for this study. Accordingly, the major microspecies of the amine group at pH 6.2 is the protonated form which makes a stronger salt bridge interaction with Asp122 (Table 1). In contrast, levels of the protonated microspecies of the amine group incrementally decrease at pH 7.2 and 8.2, weakening such an electrostatic interaction. S7911 (**3**) is an α-aminoacidic compound that, on the basis of its experimental pKa values (pKa1= 2.78 ± 0.08; pKa2= 10.49 ± 0.19), adopts a zwitterionic form as major microspecies at the investigated pH conditions. In this case, a thin effect of pH on the binding activity of **3** is only observed at pH 8.2, suggesting that raise of pH values may weaken ligand/protein electrostatic interactions. This observation can be explained by the protonation state of the piperidine ring of S7911 (**3**) which tends to be less protonated as far as the pH shift approaches the pKa of the ternary amine group (pKa2= 10.49 ± 0.19), leading to an increased fraction of the negatively charged microspecies.

Overall, MST studies suggest that presence of a net positive charge in the macrocyclic peptide (**1**) and BMS-202 (**2**) promotes binding activity to PD-L1 with decreasing pH values. This is achieved through formation and/or enforcement of salt bridge interactions with target acidic residues (Asp73 and Asp122). Moreover, this is further sustained by the lack of activity of VIS1059 (**4**), whose negative net charge and conformational restraining are detrimental for the binding activity.

Conclusions

PD-1 and PD-L1 belong to a broad family of immune checkpoint molecules which are involved in regulating T-cell activation and immune tolerance. Accordingly, they are attractive drug targets in cancer therapy because the inhibition of their interaction provides a means to remove coinhibitory signals that block antitumor immune responses. Although several humanized monoclonal antibodies targeting these immune checkpoints have been developed and are in clinical use, these biologics suffer from drug resistance and narrow therapeutic response in a majority of patients, high risk of immune-related adverse reactions, poor oral bioavailability and high costs of production. Distinct chemical classes of small molecule inhibitors of PD-1/PD-L1 interaction are being designed to tackle these limitations, though their development as novel anticancer immunotherapies still lags in preclinical settings. Recent studies support the notion that alteration of pHe and pHi in tumor microenvironment is a mechanism driving drug resistance towards anticancer therapies. In this framework, our study presented here has investigated the effect of pH shifts on the binding properties of distinct chemical classes of PD-L1 inhibitors. Results highlight the importance of pH variation in strengthening/weakening the electrostatic contribution to ligand/protein interactions of PD-L1 inhibitors. In particular, both macrocyclic peptide and small molecule inhibitors bearing a net positive charge show enhanced binding activity to the target protein with decreasing pH values, making and strengthening salt bridge interactions with acidic residues. As a consequence, decrease of pHe value below 7.0 in tumor microenvironment may enforce target engagement of PD-L1 inhibitors bearing amine groups, thus allowing escape of a tumor resistance mechanism based on acidosis. Collectively, these results provide further insights into structure-activity relationships of PD-L1 inhibitors that are useful for the design of next generation small molecule inhibitors with physicochemical properties that are resilient to variable pH conditions of tumor microenvironment.

Experimental Section

Docking Study and Molecular Dynamics. The chemical structures of PD-L1 inhibitors **1**-**3** were retrieved from PubChem (https://pubchem.ncbi.nlm.nih.gov) and compound **4** was generated using Maestro (Schrödinger Release 2019-3: Maestro, Schrödinger, LLC, New York, NY, 2019). Next, chemical structures **1**-**4** were refined using LigPrep

(Schrödinger Release 2019-3: LigPrep, Schrödinger, LLC, New York, NY, 2019) to add hydrogens, generate protonation states at pH = 7.2, and optimize their geometry using OPLS3e force field with an energy gradient convergence criterion of 0.05 kJ Å-1mol-1. Crystal structures of PD-L1 bound to peptide-57 (1, S8158; pdb code 5O4Y)[26] and BMS-202 (**2**, pdb code 5J89)[36] were downloaded from RCSB PDB (https://www.rcsb.org).[37] The crystal structure 5O4Y was split into single chain structures, keeping chain A with compound **1** bound to the GFC surface of PD-L1. In the case of crystal structure 5J89, chains C/D were kept with the co-crystallized ligand **2** bound into the cavity shaped by the GFC surface of the two PD-L1 units. The Protein Preparation Wizard (PPW)[38] tool implemented in Maestro was then employed to process and refine the selected chain structures, removing water and detergent molecules, adding hydrogen atoms and optimizing internal geometries. During geometry optimization, the OPLS3e force field was used with an atomic coordinate displacement restrain on heavy atoms set to 0.30 Å. Docking studies of compounds **3** and **4** into the binding site shaped by chains C and D of 5J89 were performed employing Glide (Schrödinger Release 2019-3: Glide, Schrödinger, LLC, New York, NY, 2019).[39] Specifically, a grid box was defined with its centre located on the centre of mass of BMS-202 (**2**) bound to chains C/D of 5J89 (x = 3.23, y = 6.18, z = 4.56). The inner grid box was sized 10 x 10 x 10 Å. Docking studies were carried out using the standard precision (SP) method and the Gscore scoring function (kcal/mol). The top scored docking pose for each molecule was selected (**3** pose #1; Gscore = -8.65 kcal/mol; **4** pose #1; Gscore = -10.04 kcal/mol), since the other remaining docking poses showed differences from that one only at level of the conformations of the solvent exposed polar group (Figures S1-S2 and Tables S1-S2, supplementary material), while presenting a conserved binding mode of the aromatic core structure. Then, the selected binding poses of compounds **3** and **4** were submitted to MD simulations, along with the refined crystallographic complexes of peptide-57 (**1**) bound to chain A of 5O4Y, and **2** bound to chains C/D of 5J89. Briefly, each PD-L1 ligand bound complex was solvated in an orthorhombic box using TIP3P water molecules, extended 10 Å away from any protein atom. The resulting system was neutralized by adding sodium and chlorine ions at a concentration of 0.15 M. Periodic boundary conditions were applied to avoid finite-size effects. Atomic partial charges of ligand were maintained as obtained from OPLS3e calculation. MD simulations were performed using Desmond (Schrödinger Release 2019-3: Desmond Molecular Dynamics System, D. E. Shaw Research, New York, NY, 2019. Maestro-Desmond Interoperability Tools, Schrödinger, New York, NY, 2019) and the OPLS3e force field.[40] The simulation protocol included starting relaxation steps and a final production phase of 50 ns. The occupancy of intermolecular and water-bridge mediated hydrogen bonds, hydrophobic contacts, aromatic (π-π stacking) and electrostatic interactions was calculated along the last 45 ns of the production phase of each MD simulation, using a cut-off value of 30% and the Simulation Interaction Diagram Tools.

Chemical compounds. Peptide-57 (S8158, **1**), BMS-202 (S7912, **2**) and S7911 (**3**) were purchased from Selleckchem (Selleckchem, Houston, USA). VIS1059 (1-(2-Methoxy-4-(2-methyl-[1,1'-biphenyl]-3-carboxamido)benzoyl)piperidine-2-carboxylic acid, **4**) was synthetized according to the following procedure.

General Methods. All the chemicals were purchased from Sigma-Aldrich (now Merck Life Science) and used without further purification. NMR spectra were recorded on a Bruker AC 400-MHz spectrometer (Bruker, Madison, WI, USA) in the indicated solvent. Chemical shifts are reported in parts per million (ppm) and are relative to $CDCl_3$ (7.26 ppm and 77.0 ppm) or CD_3OD (3.31 ppm and 49.2 ppm). The abbreviations used are as follows: s, singlet; brs, broad singlet; d, doublet; dd, double of doublets; dt, doublet of triplets; t, triplet; q, quartet; qui, quintet; m, multiplet; and brm, broad multiplet. Coupling constants (J) are reported in Hertz (Hz). Melting points were determined using a Buchi 535 electrothermal apparatus. Thin-layer chromatography (TLC) was performed on aluminium backed silica plates (silica gel 60 F254, Merck, Darmstadt, Germany). Spots were visualised by UV detector (λ: 254 nm) and/or by staining and warming with potassium permanganate. When required, flash chromatographic purifications were performed using Biotage Isolera™ Prime (Biotage AB, Uppsala, Sweden). Mass spectroscopy was performed with a Dionex UltiMate 3000 HPLC separations module combined with HCT ultra ion trap (Bruker). The analytical column was a Waters Xselect CSH Phenyl-Hexyl (5 µm, 2.1 x 150 mm), protected by a guard column 2.1 x 4 mm. Compounds purity was assessed by HPLC-DAD at 254 and 280 nm.

2-Methyl-[1,1'-biphenyl]-3-carboxylic acid (**6**).[32] To a suspension of (2-methyl-[1,1'-biphenyl]-3-yl)methanol (**5**) (1 g, 5.04 mmol) in MeCN (25 mL), $NaBrO_3$ (2.28 g, 15.13 mmol) and $NaHSO_4$ (5.04 mmol) were added at room temperature and the resulting suspension was refluxed for 1.5 h. The mixture was allowed to cool to room temperature and filtered on a pad of celite. The filtrate was concentrated under reduced pressure and the residue was redissolved in 1 M aqueous solution of NaOH (50 mL) and washed with EtOAc (3 x 20 mL). The aqueous phase was acidified with 3 N aqueous solution of HCl (pH = 3) and extracted with EtOAc (3 x 50 mL). The combined organic extracts were washed with H_2O (30 mL), brine (30 mL), dried over anhydrous Na_2SO_4 and concentrated under reduced pressure. The desired product (**6**, 750 mg, 3.53 mmol, 70% yield) was obtained as off-white solid and used for the next step without further purification. ^{1}H-NMR (400 MHz, $CDCl_3$): δ 2.47 (s, 3H), 7.22-7.31 (m, 3H), 7.34-7.36 (m, 1H), 7.39-7.44 (m, 3H), 7.99 (dd, J1= 1.36 Hz, J2= 7.79 Hz, 1H).

2-Methoxy-4-(2-methyl-[1,1'-biphenyl]-3-carboxamido)benzoic acid (**7**). To a solution of 2-methyl-[1,1'-biphenyl]-3-carboxylic acid (**6**) (750 mg, 3.53 mmol) in a mixture of dry CH_2Cl_2/DMF (1.5:1 v/v, 60 mL), $(COCl)_2$ (318 µL, 3.71 mmol) was slowly added at room temperature and under argon atmosphere. The resulting mixture was stirred at room temperature for 2 h. Volatiles were evaporated under reduced pressure and the crude acyl chloride was dissolved in dry CH_2Cl_2 (10 mL) and added dropwise to a solution of 4-amino-2-methoxybenzoic acid (562 mg, 3.36 mmol) in CH_2Cl_2 (30 mL) and Et_3N (703 µL, 5.05 mmol). The resulting mixture was stirred for 1 h at room temperature and then quenched by adding 3 N aqueous solution of HCl (20 mL). The phases were separated and the aqueous phase was extracted with CH_2Cl_2 (2 x 25 mL). The combined organic extracts were washed with H_2O (50 mL), brine (50 mL), dried over anhydrous Na_2SO_4 and concentrated under reduced pressure. The crude was purified by automated flash chromatography on silica gel (eluent: petroleum ether/EtOAc from 100:0 to 50:50, v/v) affording the desired 2-methoxy-4-(2-methyl-[1,1'-biphenyl]-3-carboxamido)benzoic acid (**7**, 100 mg, 0.28 mmol) as off-white solid. ^{1}H-NMR (400 MHz, CDCl3): δ 2.34 (s, 3H), 4.13 (s, 3H), 6.93 (dd, J1= 1.59 Hz, J2= 8.52 Hz, 1H), 7.26-7.47 (m, 7H), 8.07-8.09 (m, 2H), 8.13 (brs, 1H).

1-(2-Methoxy-4-(2-methyl-[1,1'-biphenyl]-3-carboxamido)benzoyl)piperidine-2-carboxylic acid (VIS1059, **4**). To a solution of 2-methoxy-4-(2-methyl-[1,1'-biphenyl]-3-carboxamido)benzoic acid (**7**, 80 mg, 0.22 mmol) in a mixture of dry CH_2Cl_2/DMF (1.5:1 v/v, 5 mL), $(COCl)_2$ (25 µL, 0.29 mmol) was slowly added at room temperature and under argon atmosphere. The resulting mixture was stirred at room temperature for 2 h. Volatiles were evaporated under reduced pressure and the crude acyl chloride was dissolved in dry CH_2Cl_2 (1 mL) and added dropwise to a solution pipecolic acid (30 mg, 0.23 mmol) in CH_2Cl_2 (3 mL) and Et_3N (46 µL, 0.33 mmol). The resulting mixture was stirred for 1 h at room temperature and then quenched by adding 3 N aqueous solution of HCl (5 mL). The phases were separated and the aqueous phase was extracted with CH_2Cl_2 (2 x 10 mL). The combined organic extracts were washed with H_2O (15 mL), brine (15 mL), dried over anhydrous Na_2SO_4 and concentrated under reduced pressure. The crude was purified by automated flash chromatography on silica (eluent: CH_2Cl_2/MeOH from 100:0 to 95:5, v/v) affording the desired 1-(2-methoxy-4-(2-methyl-[1,1'-biphenyl]-3-carboxamido)benzoyl)piperidine-2-carboxylic acid (VIS1059, **4**, 8 mg, 0.017 mmol) as pale yellow amorphous solid. HPLC purity (UV-DAD, 254 nm/280 nm): 94.3-94.7%. HRMS (M + H)+: m/z 473.20872 [$C_{28}H_{28}N_2O_5$ requires 472.20234], Δppm: 5.33. ^{1}H-NMR (400 MHz, CD3OD): δ 1.48-1.54 (m, 2H), 1.64-1.68 (m, 2H), 1.89 (s, 3H), 2.27-2.29 (m, 2H), 3.51-3.65 (m, 2H), 3.88 (s, 3H), 4.56-4.58 (m, 1H), 7.26-7.46 (m,

11H), 7.68 (s, 1H). ^{13}C-NMR (100.6 MHz, CD_3OD): δ 16.2, 21.2, 24.9, 29.3, 39.4, 54.7, 62.9, 102.7, 111.6, 121.7, 127.9, 125.4, 125.6, 126.8, 127.8, 127.9 (2C), 128.8 (2C), 130.9, 132.2, 138.2, 141.3, 143.2, 155.8, 168.7, 169.1, 170.2.

Physicochemical Properties. Values of cpKa for macrocyclic peptide (**1**) and small molecules (**2**-**4**) were calculated using Marvin v20.11 (ChemAxon; http://www.chemaxon.com) and Epik prediction in water solvent (Schrödinger Release 2019-3: Epik, Schrödinger, LLC, New York, NY, 2019), whereas cpKa for selected PD-L1 residues were calculated using H++ (v.3.2) server.[41-43] The pKa plugin of Marvin calculates pKa values of compounds based on the partial charge distribution of the small molecule, whereas Epik uses Hammett and Taft methods for pKa prediction in water or DMSO solvent.[44] It is worth noting that, in both cases, significant differences were observed between predicted and experimental pKa values of compounds **2**-**4** (Table 2). Experimental acidic constant (pKa) of compounds **2**-**4** were determined using Pion Sirius T3 instrument. Each experiment was performed in triplicate, specifying sample weight, number of expected pKa values, predicted pKa values, and titration mode. In order to measure the pKa of a compound, a sample concentration of 1 mM was prepared. Poor soluble compounds (**2**, **4**) were dissolved adding methanol as co-solvent. In this case, three titrations were performed at different methanol/water ratios (from 60:40 to 40:60, v/v)) in order to determine aqueous pKa. The Yasuda-Shedlovsky method was chosen to extrapolate aqueous pKa values. The R^2 value was used to evaluate the validity of the assay with co-solvent, and results were considered acceptable with R^2 value ≥ 0.9. Conversely, root mean square deviation (RMSD) value from the theoretical curve was used to assess the quality of experiments performed for compound **3** dissolved without co-solvent. Results were analyzed using Sirius T3 software v1.1.0.5.

Microscale Thermophoresis (MST). Recombinant human extracellular domain of PD-L1 (wt-hPD-L1; cat. n. ab167713, 26 kDa) was purchased from Abcam (Abcam, Cambridge, UK). wt-hPD-L1 was reconstituted following Abcam's protocol, adding sterile water to reach the final theoretical concentration of 0.1 mg/0.32 ml. The protein amount was assessed on the basis of its absorbance at 205 nm (ε = 31 M^{-1} cm^{-1})[45] as determined with NanoDrop-One spectrophotometer (v.1.3), yielding a concentration of 12 µM. The protein was first labelled at pH 7.2 using the protein labelling kit NT650 red-NHS 2nd generation dye supplied by NanoTemper (MO-L011; NanoTemper Technologies, Munich, Germany), using a 1:4 protein to dye ratio. Specifically, a volume of 100 µL of 12 µM solution of wt-hPD-L1 protein in phosphate buffer ($PB_{7.2}$: 50 mM KH_2PO_4, 0.05% Tween 20, pH 7.2) was mixed with 100µL of 48µM NT650-NHS fluorophore in $PB_{7.2}$, and incubated for 30 minutes at room temperature (RT) in the dark. Then, unbounded fluorophore was removed by size-exclusion chromatography column using $PB_{7.2}$ buffer as storage buffer. We determined the labelled protein concentration by UV-measurement. Specifically, the degree of labeling of protein (DoL) was 0.27. This value was determined using the protein extinction coefficient ε_{205nm} = 31 M^{-1} cm^{-1}, dye ε_{650nm} = 195,000 $M^{-1}cm^{-1}$, a correcting factor at 205nm (cf_{205nm}) = 0.19, and employing equations 1-3:

eq.1 $C_{prot} = [A_{205} – (A_{650} \times cf) / 31\ M^{-1}\ cm^{-1} \times MW]$,

eq.2 $C_{dye} = [A_{650} / 195{,}000\ M^{-1}\ cm^{-1} \times l]$,

eq.3 $DoL = C_{dye}/C_{prot}$

In order to investigate binding properties of compounds to PD-L1 at pH 6.2 and 8.2, the removal of unbounded fluorophore after labelling reaction was performed using size-exclusion chromatography column conditioned with two different phosphate buffers ($PB_{6.2}$: 50 mM KH_2PO_4, 0.05% Tween 20, pH 6.2; $PB_{8.2}$: 50 mM KH_2PO_4, 0.05% Tween 20, pH 8.2). Specifically, the labelled protein solution was split into two columns and then eluted using $PB_{6.2}$ and $PB_{8.2}$, respectively. The DoL was determined for each collected solution, yielding in both cases a value of 0.34. Pre-dilutions of compounds (**1**-**4**) were prepared for MST experiments by 16-fold 1:1 serial dilution in running buffer, such as PB at the selected pH containing 4% DMSO in PCR tubes supplied by NanoTemper Technologies to yield final volumes of 10 µL. In particular, compounds were tested in triplicate using different concentrations for each compound, starting from 0.1 mM for peptide-57 (**1**), 0.5 mM for BMS-202 (**2**), 1 mM for S7911 (**3**), 1 mM for VIS1059 (**4**). An amount of 10 µl solution of 100 nM red-hPD-L1 was added to each compound dilution and mixed to halve the concentration of each component, including 2% DMSO and a reaction volume of 20 µL. These samples were loaded into 16 premium-coated capillary tubes (MO-K025; NanoTemper Technologies, Munich, Germany) and inserted in the chip tray of Monolith NT.115 for thermophoresis analysis. Compounds **1**-**4** were tested with labeled protein at pH 7.2, whereas only active compounds (**1**-**3**) were also tested with labeled protein at pH 6.2 and pH 8.2. Capillary tubes were illuminated with an infrared laser to generate a temperature gradient. The diffusion of ligand/protein complex was monitored along the temperature gradient through the measurement of fluorescence intensity in each capillary tube. MST signals were recorded at medium laser power for small molecules **2**-**4**, whereas high laser power was used for the macrocyclic peptide (**1**). A led power of 40% was used for all compounds 1-4. Dissociation constants (K_d) were extrapolated by ligand concentration-dependent changes of red-hPD-L1 normalized fluorescence (F_{norm}). Raw data were analyzed with the MO.Affinity Analysis software v2.3 in manual mode setting the hot region at time 19/20s for small molecules (**2**-**4**) and 9/10s for macrocycle peptide (**1**). Confidence values (c.v., ±) are reported next to K_d values, indicating the range where the K_d falls with a 68% of certainty.

Label-free thermal shift analysis. The stability of red-hPD-L1 protein at different pH after labelling procedure was checked using label-free thermal shift analysis with Tycho instrument (NT.6; NanoTemper Technologies, Munich, Germany). Specifically, label-free thermal shift analysis monitors changes in emission intensity and wavelength maximum of intrinsic fluorescence properties of buried Trp and Tyr residues in protein that become exposed in the unfolded state when the protein is exposed to an increasing temperature range from 35°C to 95°C. wt-hPD-L1and red-hPD-L1 from labelling processes at pH 6.2, 7.2 and 8.2 were diluted in the relative PB ($PB_{6.2}$, $PB_{7.2}$, $PB_{8.2}$) at concentration of 2.7 µM. Samples were loaded into Tycho NT.6 capillaries (TY-C001; NanoTemper Technologies, Munich, Germany) and the thermal unfolding profiles for wt-hPD-L1 and red-hPD-L1 were recorded. Experiments were carried out in triplicate and inflection temperature (Ti) values are reported as mean ± standard deviation values (Figure S3 and Table S3, supplementary material). As a result, no shift of unfolding temperature (ΔTi < 1.0) was observed between unlabeled wt-hPD-L1 and red-hPD-L1 at pH 6.2, pH 7.2 and pH 8.2. This observation suggests that labelling process and pH values do not affect the stability of the protein.

Acknowledgements

This work was supported by Sterling S.p.A and PO FSE Umbria 2014-2020, D.D. n. 3806 20/04/2018. AC acknowledges a research grant fellowship (PO FSE Umbria 2014-2020, D.D. n. 3806 20/04/2018).

Supporting Information

Figure S1: solutions (#1-4, Table S1) of the docking pose of compound **3** (S7911) into the binding cleft of the dimeric form of PD-L1 (5J89). Figure S2: solutions (#1-4, Table S2) of the docking pose of compound **4** (VIS1059) into the binding cleft of the dimeric form of PD-L1 (5J89). Figure S3: unfolding profile of wt-hPD-L1 (wild type) and red-hPD-L1 (RED pH 6.2; RED pH 7.2; RED pH 8.2) at different pH conditions. Table S1: energetic scores

(Gscore, kcal/mol) and root mean square deviation (RMSD, Å) of docking poses of compound **3** (S7911) into the binding cleft of the dimeric form of PD-L1 (5J89). Table S2: energetic scores (Gscore, kcal/mol) and root mean square deviation (RMSD, Å) of docking poses of compound **4** (VIS1059) into the binding cleft of the dimeric form of PD-L1 (5J89). Table S3: inflection temperature (Ti), initial ratio and Δratio of wt-hPD-L1 and red-hPD-L1 at different pH conditions.

Keywords: Immunotherapy • Check-point inhibitors • Thermophoresis • Molecular dynamics • Cancer

References:

[1] G.J. Freeman, A.J. Long, Y. Iwai, K. Bourque, T. Chernova, H. Nishimura, L.J. Fitz, N. Malenkovich, T. Okazaki, M.C. Byrne, H.F. Horton, L. Fouser, L. Carter, V. Ling, M.R. Bowman, B.M. Carreno, M. Collins, C.R. Wood, T. Honjo, *J. Exp. Med.* **2000**, *192*, 1027–34. https://doi.org/10.1084/jem.192.7.1027.

[2] Y. Latchman, C.R. Wood, T. Chernova, D. Chaudhary, M. Borde, I. Chernova, Y. Iwai, A.J. Long, J.A. Brown, R. Nunes, E.A. Greenfield, K. Bourque, V.A. Boussiotis, L.L. Carter, B.M. Carreno, N. Malenkovich, H. Nishimura, T. Okazaki, T. Honjo, A.H. Sharpe, G.J. Freeman, *Nat. Immunol.* **2001**, *2*, 261–268. https://doi.org/10.1038/85330.

[3] V.A. Boussiotis, *N. Engl. J. Med.* **2016**, *375*, 1767–1778. https://doi.org/10.1056/NEJMra1514296

[4] B.M. Carreno, M. Collins, *Annu. Rev. Immunol*. **2002** *20*, 29–53. https://doi.org/10.1146/annurev.immunol.20.091101.091806.

[5] E.O. Long, *Annu. Rev. Immunol*. **2002**, *17*, 875–904. https://doi.org/10.1146/annurev.immunol.17.1.875.

[6] Y. Agata, A. Kawasaki, H. Nishimura, Y. Ishida, T. Tsubata, H. Yagita, T. Honjo, *Int. Immunol.* **1996**, *8*, 765–72. http://www.ncbi.nlm.nih.gov/pubmed/8671665.

[7] H. Nishimura, Y. Agata, A. Kawasaki, M. Sato, S. Imamura, N. Minato, H. Yagita, T. Nakano, T. Honjo, *Int. Immunol*. **1996**, *8*, 773–80. https://doi.org/10.1093/intimm/8.5.773.

[8] M. Collins, V. Ling, B.M. Carreno, *Genome Biol*. **2005,** *6*, 1–7. https://doi.org/10.1186/gb-2005-6-6-223.

[9] K.M. Zak, P. Grudnik, K. Magiera, A. Dömling, G. Dubin, T.A. Holak, *Structure.* **2017**, *25*, 1163–1174. https://doi.org/10.1016/j.str.2017.06.011.

[10] S. Tang, P.S. Kim, *Proc. Natl. Acad. Sci. USA*. **2019**, *116*, 24500-24506. https://doi.org/10.1073/pnas.1916916116.

[11] D.Y. Lin, Y. Tanaka, M. Iwasaki, A.G. Gittis, H.-P. Su, B. Mikami, T. Okazaki, T. Honjo, N. Minato, D.N. Garboczi, *Proc. Natl. Acad. Sci. USA*. **2008**, *105*, 3011-3016. https://doi.org/10.1073/pnas.0712278105.

[12] X. Cheng, V. Veverka, A. Radhakrishnan, L.C. Waters, F.W. Muskett, S. H. Morgan, J. Huo, C. Yu, E.J. Evans, A. J. Leslie, M. Griffiths, C. Stubberfield, R. Griffin, A.J. Henry, A. Jansson, J.E. Ladbury, S. Ikemizu, M.D. Carr, *J. Biol. Chem*. **2013,** *288*, 11771-11785. https://doi.org/10.1074/jbc.M112.448126.

[13] K. M. Zak, R. Kitel, S. Przetocka, P. Golik, K. Guzik, B. Musielak, A. Dömling, G. Dubin, T.A. Holak, *Structure*. **2015,** *23*, 2341-2348. https://doi.org/10.1016/j.str.2015.09.010.

[14] M. Ghiotto, L. Gauthier, N. Serriari, S. Pastor, A. Truneh, J.A. Nunè, D. Olive, *Int. Immunol*. **2010,** 22, 651–660. https://doi.org/10.1093/intimm/dxq049.

[15] T. Yamazaki, H. Akiba, H. Iwai, H. Matsuda, M. Aoki, Y. Tanno, T. Shin, H. Tsuchiya, D.M. Pardoll, K. Okumura, M. Azuma, H. Yagita, *J. Immunol*. **2002** 169, 5538–45. https://doi.org/10.4049/jimmunol.169.10.5538.

[16] X. Jiang, J. Wang, X. Deng, F. Xiong, J. Ge, B. Xiang, X. Wu, J. Ma, M. Zhou, X. Li, Y. Li, G. Li, W. Xiong, C. Guo, Z. Zeng, *Mol. Cancer*. **2019**, *18*, 1–17. https://doi.org/10.1186/s12943-018-0928-4.

[17] D. F. Quail, J. A. Joyce, *Nat. Med*. **2013**, *19*, 1423-1437. 10.1038/nm.3394. https://doi.org/10.1038/nm.3394.

[18] T. Chen, Q. Li, Z. Liu, Y. Chen, F. Feng, H. Sun, *Eur. J. Med. Chem*. **2019**, *161*, 378–398. https://doi.org/10.1016/j.ejmech.2018.10.044.

[19] J.M. Taube, A.J. Korman, S.N. Gettinger, J.D. Powderly, G.D. Kollia, R.A. Anders, S.J. Antonia, M. Jure-Kunkel, R.D. Carvajal, P.D. Leming, L. Chen, J.M. Wigginton, J.R. Brahmer, H. Xu, T.L. McMiller, S. Agrawal, D.M. Pardoll, D.C. Smith, S.L. Topalian, F.S. Hodi, W.H. Sharfman, C.G. Drake, J.A. Sosman, D. McDonald, L. Horn, M.B. Atkins, M. Sznol, A. Gupta, D.R. Spigel, D.F. McDermott, *N. Engl. J. Med*. **2012**, *366*, 2443–2454. https://doi.org/10.1056/nejmoa1200690.

[20] Y. Chen, Y. Pei, J. Luo, Z. Huang, J. Yu, X. Meng, *Front. Immunol*. **2011** *11*, 1088. https://doi.org/10.3389/fimmu.2020.01088.

[21] H. Zhu, C. Du, M. Yuan, P. Fu, Q. he, B. Yang, J. Cao, *Drug Discov. Today* **2020**, *20*, 30265-8. https://doi.org/10.1016/j.drudis.2020.07.006.

[22] R.S. Herbst, J.-C. Soria, M. Kowanetz, G.D. Fine, O. Hamid, M.S. Gordon, J.A. Sosman, D.F. Mcdermott, J.D. Powderly, S.N. Gettinger, H.E.K. Kohrt, L. Horn, D.P. Lawrence, S. Rost, M. Leabman, Y. Xiao, A. Mokatrin, H. Koeppen, P.S. Hegde, I. Mellman, D.S. Chen, F.S. Hodi, *Nature* **2014**, *515*, 563–567. https://doi.org/10.1038/nature14011.

[23] C. Corbet, O. Feron, *Nat. Rev. Cancer*. **2017**, *17*, 577–593. https://doi.org/10.1038/nrc.2017.77.

[24] B.A. Webb, M. Chimenti, M.P. Jacobson, D.L. Barber, *Nat. Rev. Cancer* **2011**, *11*, 671–677. https://doi.org/10.1038/nrc3110.

[25] D.E. Korenchan, R.R. Flavell, *Cancers (Basel).* **2019**, *11*, 1026. https://doi.org/10.3390/cancers11071026.

[26] J.E. Ippolito, M.W. Brandenburg, X. Ge, J.R. Crowley, K.M. Kirmess, A. Som, D.A. D'Avignon, J.M. Arbeit, S. Achilefu, K.E. Yarasheski, J. Milbrandt, *PLoS ONE*, **2016**, *11*, e0159675. https://doi.org/10.1371/journal.pone.0159675.

[27] N. Raghunand, X. He, R. Van Sluis, B. Mahoney, B. Baggett, C.W. Taylor, G. Paine-Murrieta, D. Roe, Z.M. Bhujwalla, R.J. Gillies, *Br. J. Cancer* **1999**, *80*, 1005–1011. https://doi.org/10.1038/sj.bjc.6690455.

[28] H.X. Zhou, X. Pang, *Chem. Rev*. **2018**, *118*, 1691–1741. https://doi.org/10.1021/acs.chemrev.7b00305.

[29] K. Magiera-Mularz, L. Skalniak, K.M. Zak, B. Musielak, E. Rudzinska-Szostak, Ł. Berlicki, J. Kocik, P. Grudnik, D. Sala, T. Zarganes-Tzitzikas, S. Shaabani, A. Dömling, G. Dubin, T.A. Holak, *Angew. Chem. Int. Ed. Engl.* **2017**, *56,* 13732–13735. https://doi.org/10.1002/anie.201707707.

[30] X. Chupak, L. S.; Zheng, Compounds Useful as Immunomodulators, WO2015034820, Bristol-Myers Squibb Company, US, 2015.

[31] K. M. Zak, P. Grudnik, K. Guzik, B.J. Zieba, B. Musielak, A. Dömling, G. Dubin, T.A. Holak, *Oncotarget.* **2016**, *7*, 30323–30335. https://doi.org/10.18632/oncotarget.8730.

[32] S. Ueno, M. Ohtsubo, R. Kuwano, [4+2] Cycloaddition of o-xylylenes with imines using palladium catalyst. *J. Am. Chem. Soc.* **2009**, *131*, 12904–12905. https://doi.org/10.1021/ja905988e.

[33] S. Duhr, D. Braun, *Proc. Natl. Acad. Sci. USA.* **2006**, *103*, 19678–19682. https://doi.org/10.1073/pnas.0603873103.

[34] A. Ganesan, M. Ahmed, I. Okoye, E. Arutyunova, D. Babu, W.L. Turnbull, J.K. Kundu, J. Shields, K.C. Agopsowicz, L. Xu, Y. Tabana, N. Srivastava, G. Zhang, T.C. Moon, A. Belovodskiy, M. Hena, A.S. Kandadai, S.N. Hosseini, M. Hitt, J. Walker, M. Smylie, F.G. West, A.G. Siraki, M.J. Lemieux, S. Elahi, J.A. Nieman, D.L. Tyrrell, M. Houghton, K. Barakat, *Sci. Rep.* **2019**, *9*, 12392. https://doi.org/10.1038/s41598-019-48826-6.

[35] A. Macchiarulo, R. Pellicciari, *J. Mol. Graph. Model.* **2007**, *26*, 728–739. https://doi.org/10.1016/j.jmgm.2007.04.010.

[36] K. M. Zak, P. Grudnik, K. Guzik, B. J. Zieba, B. Musielak, A. Dömling, G. Dubin, T. A. Holak, *Oncotarget*. **2016**, *7*, 30323–30335. https://doi.org/10.18632/oncotarget.8730.

[37] H. M. Berman, T. Battistuz, T. N. Bhat, W. F. Bluhm, P. E. Bourne, K. Burkhardt, Z. Feng, G. L. Gilliland, L. Iype, S. Jain, P. Fagan, J. Marvin, D. Padilla, V. Ravichandran, B. Schneider, N. Thanki, H. Weissig, J. D. Westbrook, C. Zardecki, *Acta Crystallogr. D Biol. Crystallogr.* **2002**, *58*, 899–907. https://doi.org/10.1107/S0907444902003451.

[38] G. Madhavi Sastry, M. Adzhigirey, T. Day, R. Annabhimoju, W. Sherman, *J. Comput. Aided. Mol. Des*. **2013**, *27*, 221–234. https://doi.org/10.1007/s10822-013-9644-8.

[39] R.A. Friesner, J.L. Banks, R.B. Murphy, T.A. Halgren, J.J. Klicic, D.T. Mainz, M.P. Repasky, E.H. Knoll, M. Shelley, J.K. Perry, D. E. Shaw,

Perry Francis, P. S. Shenkin, *J. Med. Chem*. **2004**, *47*, 1739-1749. https://doi.org/10.1021/JM0306430.

[40] K. J. Bowers, E. Chow, H. Xu, R. O. Dror, M. P. Eastwood, B. A. Gregersen, J. L. Klepeis, I. Kolossvary, M. A. Moraes, F. D. Sacerdoti, J. K. Salmon, Y. Shan, D. E. Shaw, ACM/IEEE Conf. Supercomput, ACM Press, New York, USA, **2006**, *84*. https://doi.org/10.1145/1188455.1188544.

[41] R. Anandakrishnan, B. Aguilar, A. V Onufriev, *Nucleic Acids Res.* **2012**, *40*, W537-W541. https://doi.org/10.1093/nar/gks375.

[42] J.C. Gordon, J.B. Myers, T. Folta, V. Shoja, L.S. Heath, A. Onufriev, *Nucleic Acids Res.*, **2005**, *33*, W368-W371. https://doi.org/10.1093/nar/gki464.

[43] J. Myers, G. Grothaus, S. Narayanan, A. Onufriev, *Proteins*. **2006**, *63*, 928–938. https://doi.org/10.1002/prot.20922.

[44] J.C. Shelley, A. Cholleti, L. Frye, J.R. Greenwood, M.R. Timlin, M. Uchimaya, *J. Comp. Aided Mol. Des.* **2007**, 21, 681-691. https://doi.org/10.1007/s10822-007-9133-z.

[45] R. K. Scopes, *Anal. Biochem*. **1974**, *59*, 277–282. https://doi.org/10.1016/0003-2697(74)90034-7.

Entry for the Table of Contents

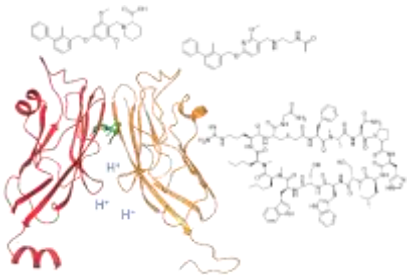

While inhibitors of PD-1/PD-L1 interaction are being developed as anticancer immunotherapies, alteration of pH in the tumor microenvironment is thought to promote drug resistance. In this study, we show that pH variation affects dissociation constants of PD-L1 inhibitors, influencing polar interactions. Results suggest that a decrease of pH may enforce target engagement of PD-L1 inhibitors bearing amine groups, thereby allowing to escape acidosis as tumor resistance mechanism.